Journal of Microscopy, Vol. 211, Pt 2 August 2003, pp. 154–160
Received 27 January 2003; accepted 8 May 2003

Wavelet-based image restoration for compact X-ray microscopy

H. STOLLBERG, J. BOUTET DE MONVEL*, A. HOLMBERG & H. M. HERTZ
Biomedical & X-ray Physics, Royal Institute of Technology/SCFAB, SE-10691, Stockholm, Sweden
**Center for Hearing and Communication Research and Department of Clinical Neuroscience, Karolinska Institute, SE-17176 Stockholm, Sweden*

Key words. Compact X-ray microscopy, image restoration, wavelet denoising.

Summary

Compact water-window X-ray microscopy with short exposure times will always be limited on photons owing to sources of limited power in combination with low-efficency X-ray optics. Thus, it is important to investigate methods for improving the signal-to-noise ratio in the images. We show that a wavelet-based denoising procedure significantly improves the quality and contrast in compact X-ray microscopy images. A non-decimated, discrete wavelet transform (DWT) is applied to original, noisy images. After applying a thresholding procedure to the finest scales of the DWT, by setting to zero all wavelet coefficients of magnitude below a prescribed value, the inverse DWT to the thresholded DWT produces denoised images. It is concluded that the denoising procedure has potential to reduce the exposure time by a factor of 2 without loss of relevant image information.

1. Introduction

Recent progress in soft X-ray optics and sources has allowed the development of compact soft X-ray microscopes. Unfortunately, imaging with such microscopes still provides noisy images or requires long exposure times, owing to the limited power of compact sources and inefficient optics. In the present paper we demonstrate that denoising by a wavelet-based algorithm results in an improvement in image quality without loss of relevant image information.

Soft X-ray microscopy in the water-window region ($\lambda = 2.3$–4.4 nm; approximately 0.3–0.5 keV) is an attractive technique for high-resolution biological imaging owing to the possibility of studying thick unstained objects in an aqueous environment (Schmahl *et al.*, 1980; Kirz *et al.*, 1995). Such microscopes rely on powerful contrast mechanisms between water and a number of elements, e.g. carbon, silicon and others, because of the low absorption of water in this spectral region. Current operational X-ray microscopes are based on synchrotron radiation sources, which unfortunately limit the accessibility and thus applicability for, e.g. biological research. We have developed the first compact X-ray microscope with a liquid-jet laser-plasma source (Berglund *et al.*, 2000; Johansson *et al.*, 2002). Such a table-top microscope shows promise for use in the small-to-medium-scale application laboratory, thereby increasing the impact of X-ray microscopy.

Different image restoration methods have been designed and tested over the years in the field of microscopy. In X-ray microscopy, however, only few attempts to improve the images have been reported (Sibarita *et al.*, 1995, 1998; Lehr *et al.*, 1998). In these studies, different algorithms were applied to images recorded at synchrotron-based X-ray microscopes. By contrast to our compact microscope, such instruments provide images with good signal-to-noise ratio (S/N) as a result of the high photon flux of the sources. Typically, such microscopes record 10^3 photons per resolution element in a few seconds at $1000\times$ magnification. In the compact microscope, the lower photon flux of our laser-plasma source results in a limited S/N, especially at short exposure times. Currently we record 5–50 photons/resolution element in a 30-s exposure, depending on which optics we use. Because noise is basically Poisson distributed [$S/N = 1/\sqrt{(N)}$], it is clear that efficient denoising methods are very important to improve image quality. In this paper we have investigated a denoising procedure based on the wavelet transform.

Algorithms based on the discrete wavelet transform have been used in recent years to estimate a signal from blurred and noisy data (Donoho & Johnstone, 1994, 1995; Starck & Bijaoui, 1994; Donoho, 1995). Wavelet-based processing has been applied to the wide range of one-dimensional (1D) to 3D imaging and data analysis, e.g. analysis of spectra (Fligge & Solanki, 1997), restoration of astronomical images (Starck *et al.*, 1994) or confocal microscopy (Boutet de Monvel *et al.*, 2001). Compared with, for example, classical Fourier methods, which provide denoising based on the overall frequency

Correspondence: Heide Stollberg. Tel.: +46 (0)8 55378126; fax: +46 (0)8 55378466; e-mail: heide.stollberg@biox.kth.se

content in the image, the wavelet methods are based on information about the spatial frequency content, which is coupled to the position in the image. Thus, the denoising parameters can be estimated and selected more locally. This is suitable for X-ray microscopy images with highly variable contrast and spatial frequencies in different parts of the image. In the present article we apply wavelet processes to X-ray microscopy and demonstrate that it is possible to reduce noise corresponding to a decrease in the exposure time by a factor of 2 without loss of relevant image information. To our knowledge, this is the first time wavelet processes have been applied to X-ray microscopy, and the first time that compact X-ray microscope images have been improved by image processing.

We first describe the Stockholm compact X-ray microscope, which provides all our images. In a second step we explain the theoretical basis and describe the application of wavelet-based denoising. Finally we discuss the results of the denoising algorithm and show some images of test samples.

2. Experimental arrangement of the compact X-ray microscope

The compact full-field X-ray microscope (Berglund *et al.*, 2000; Johansson *et al.*, 2002) is based on a 100-Hz, negligible-debris, high-brightness ethanol liquid-jet laser-plasma source providing $\lambda = 3.37$ nm radiation from carbon-ion emission with narrow line width ($\lambda/\Delta\lambda > 500$) (Wilhein *et al.*, 1997). The source is combined with a spherical W/B_4C normal-incidence multilayer mirror, which operates as condenser. In the present paper the high-resolution imaging is performed with a nickel zone plate with an outermost zone width of 40 nm. Detection is performed with a back-illuminated CCD camera, with a pixel size of 24×24 nm^2 in the object plane at 1000× magnification (Fig. 1).

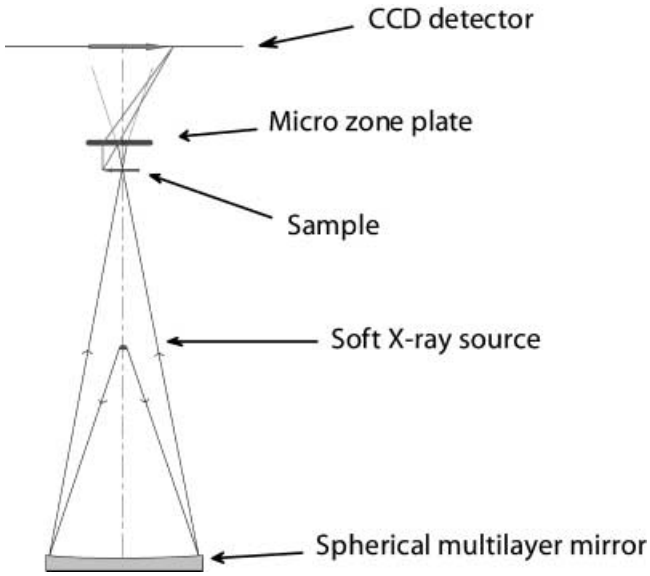

Fig. 1. Schematic experimental arrangement of the compact X-ray microscope.

3. Wavelet-based denoising

3.1. Introduction

When denoising images containing structures of different shapes and sizes, it is advantageous to treat different spatial frequencies or scales separately. In the wavelet analysis a scale parameter j, defined as the inverse of some local spatial frequency of the signal, is used rather than the global spatial frequency of the Fourier transform (Mallat, 1999). With wavelet analysis it is possible to analyse and process a signal in a position- and scale-dependent way.

The basic scheme for multiscale analysis is the repeated application of two conjugate scaling transformations on the signal I, $I(x) \rightarrow L{\cdot}I(x)$ and $I(x) \rightarrow H{\cdot}I(x)$ with a low-pass filter L and a high-pass filter H. The repeated application of L allows us to work on coarser and coarser resolution and H allows us to keep track of information when passing from one scale to the next. A method of implementing this scheme in a non-redundant way is the discrete wavelet transform (DWT) (Mallat, 1999), which is discussed below in Section 3.2. In this transform the information extracted at different scales and different positions represents independent components of the image. The wavelet-based denoising (Donoho & Johnstone, 1994) uses these properties of the DWT to recover a signal degraded by noise. The DWT is applied to the signal and a certain thresholding (cf. Section 3.3) is performed in the wavelet domain. By this thresholding, only significant wavelet coefficients remain, and the application of the inverse DWT results in a denoised image. For our experiments we applied the SURE wavelet shrinkage procedure of Donoho (1995), which is briefly described in a more formal way in Section 3.3.

Because the noise is primarily concentrated in the finer scales, and significant data typically involve sets of high-level wavelet coefficients, these significant data are mostly unaffected by the denoising procedure. The algorithm produces an adaptive smoothing of the image with strongly suppressed noise, and sharp features are preserved. It has been shown that the wavelet-denoising algorithm as described above often outperforms the more classic denoising methods based on linear filtering (Donoho & Johnstone, 1994; Mallat, 1999).

3.2. Discrete wavelet transform

In our experiments the discrete transform analogous to the continous wavelet transform was used (Mallat, 1999). This transform is based on a discrete scaling function Φ_{j_0} and discrete wavelet functions Ψ_j^a. The translation-invariant DWT is obtained by using discrete convolutions of the original image $I(x)$ with Φ_{j_0} and Ψ_j^a.

$$I_{j_0}(x) = \Phi_{j_0} * I(x),\ w_j^a(x) = \Psi_{j_0}^a * I(x) \quad (j = 1, \ldots, j_0,\ 1 \le a \le 3) \tag{1}$$

where * denotes the cyclic convolution of two arrays, $w_j^a(x)$ are the wavelet coefficients, j labels the wavelet scales, and a labels the different wavelet filters. The transform can be inverted by

$$I(x) = 2^{-2j_0}\check{\Phi}_{j_0} * I_{j_0}(x) + \sum_{j=1}^{j_0}\sum_{a} 2^{-2j}\check{\Psi}_j^a * w_j^a(x) \tag{2}$$

with $\check{f}(x) = f(-x)$. The scaling and wavelet functions used are constructed from filters associated with 1D Daubechies' wavelets for each axis x and y (Mallat, 1999).

3.3. Wavelet denoising

The denoising was performed with the wavelet shrinkage method (Donoho & Johnstone, 1994). The principle is to choose a threshold value $T_i^a > 0$ and to replace the wavelet coefficients $w_j^a(x)$ by their soft-thresholded estimate $\hat{w}_j^a$:

$$\hat{w}_j^a(x \mid T_j^a) = 0 \qquad \text{if} \quad |w_j^a(x)| < \mathrm{T} \tag{3}$$

$$\hat{w}_j^a(x \mid T_j^a) = w_j^a(x) - \mathrm{sgn}(w_j^a(x))T_j^a \quad \text{if} \quad |w_j^a(x)| > \mathrm{T} \tag{4}$$

To choose the thresholds, one has to estimate the mean-square error Err(T) for a given threshold T:

$$Err = \sum_x (\hat{w}_j^a(I(x \mid T_j^a)) - w_j^a(I_0(x)))^2 \tag{5}$$

If one knows the distribution of the noise, it is possible to write a general unbiased estimate of Err(T), called the Stein's unbiased risk estimate (SURE). The minimization of Err_{SURE}(T) over T leads to a choise of T_j^a, which becomes optimal in the limit of large images (Donoho & Johnstone, 1995). For noise following Poisson statistics, which is basically the case for compact X-ray microscope images, the SURE method works reasonably well if applied on relatively uniform parts of the image.

4. Restoration of images

The purpose of these experiments was to observe the results of the restoration and to optimize the restoration parameters.

The objects used to test and optimize the denoising algorithm are gratings with a well-defined grating period. They are manufactured in nickel on a silicon nitride substrate employing a nano-lithography technique. A tri-layer resist system with underlying plating base is prepared on a silicon nitride substrate. The resist system is structured with e-beam lithography and reactive ion etching to form a plating mould. Nickel is then electroplated into the mould and finally the mould is removed by reactive ion etching. With this technique we have fabricated gratings with 50-nm period, which is below the current resolution limit of the microscope. The thicknesses of the nickel structures are typically 100–130 nm, corresponding to an absorption of 65–75% at the operating wavelength of 3.37 nm.

Figure 2(a) shows the initial image of a hyperbolic grating, averaged over three 7-s exposures with 1000× magnification. The smallest structure has a size of about 80 nm. The images in Fig. 2(b–d) are the restored averaged images for different scale levels. For the images in Fig. 2(b,c), there is an increased S/N compared with the initial image in Fig. 2(a). The smaller structures are more clearly visible than in the initial image. In the image on the lower right (Fig. 2d), however, one can see the loss of information for smaller structure width when applying the thresholding also on the third scale level.

Figure 3 shows a grating with 120 nm period and a line-to-space ratio of 1 : 1 at 1000× magnification. Figure 3(a) is the initial image obtained at 5 s exposure time, and Fig. 3(b,c) show the restored image after thresholding at the first scale level and at the first and second scale levels, respectively. Figure 3(d) is an image of the same grating, obtained with 30 s exposure time. Comparing the images in Fig. 3(a,b), one can see a clear improvement of the S/N without loss of information. Figure 3(b,d) seem to have the same visual image quality.

Although visual impression of improved image quality is an important criterion, a more quantitative method is preferable. Figure 4 shows the power spectra for the four images in Fig. 3. The double peak, marked by arrows, in the power spectra represents the major spatial frequencies in the grating structure. As one can see, the soft-thresholding reduces the signal for higher spatial frequencies, i.e. the noise, without changing the significant data (curve b), whereas a second application of the thresholding at the next scale level causes a loss in significant data (curve c).

For most applications it is sufficient to use the mean-square thresholds computed for the different scales, and to weigh these thresholds equally in order to optimize the restoration. With this procedure we could limit ourselves to the first two scale levels in the wavelet transform. Thresholding of the third and coarser scales causes a loss of information in the smaller structures near the resolution limit, as illustrated in Figs 2 and 4. Therefore, depending on the structure size, we applied the thresholding on one or two scale levels.

To show the difference to conventional Fourier methods we applied a pixel-wise adaptive Wiener filtering to the grating in Fig. 3 (Matlab Image Processing Toolbox, http://www.mathworks.com). This Wiener filtering method is based on statistics estimated from a local neighbourhood of each pixel. In the following we discuss the Wiener filtering using two and three pixels in the neighbourhood. In Fig. 5 the power spectra for the initial image (curve a) and the two- and three-pixel Wiener-filtered images are shown (curves b and c, respectively). For comparison, curve d shows the power spectrum for the wavelet-denoised image. It is obvious that the Wiener filtering using the two-pixel neighbourhood (curve b) gives about the same values for spatial frequencies of interest

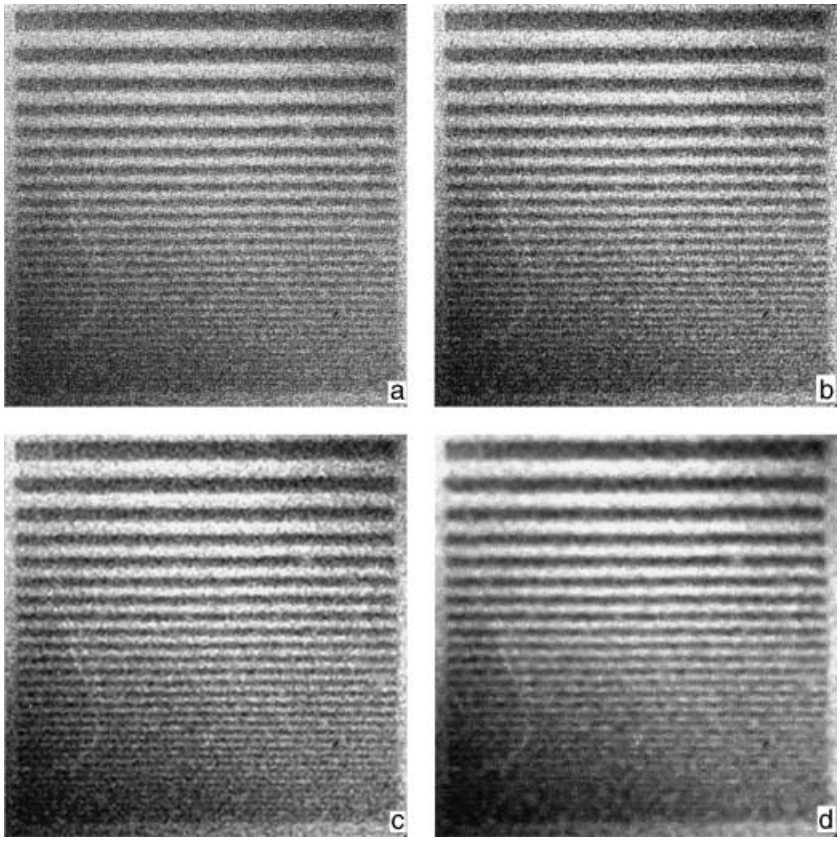

Fig. 2. Compact X-ray microscope image of a hyperbolic grating, taken at $\lambda = 3.37$ nm. (a) The original image, averaged over three images acquired with 7 s exposure time. (b–d) Results of the restoration process on the image a for thresholding at different scale levels. The line width varies from 600 nm to 80 nm.

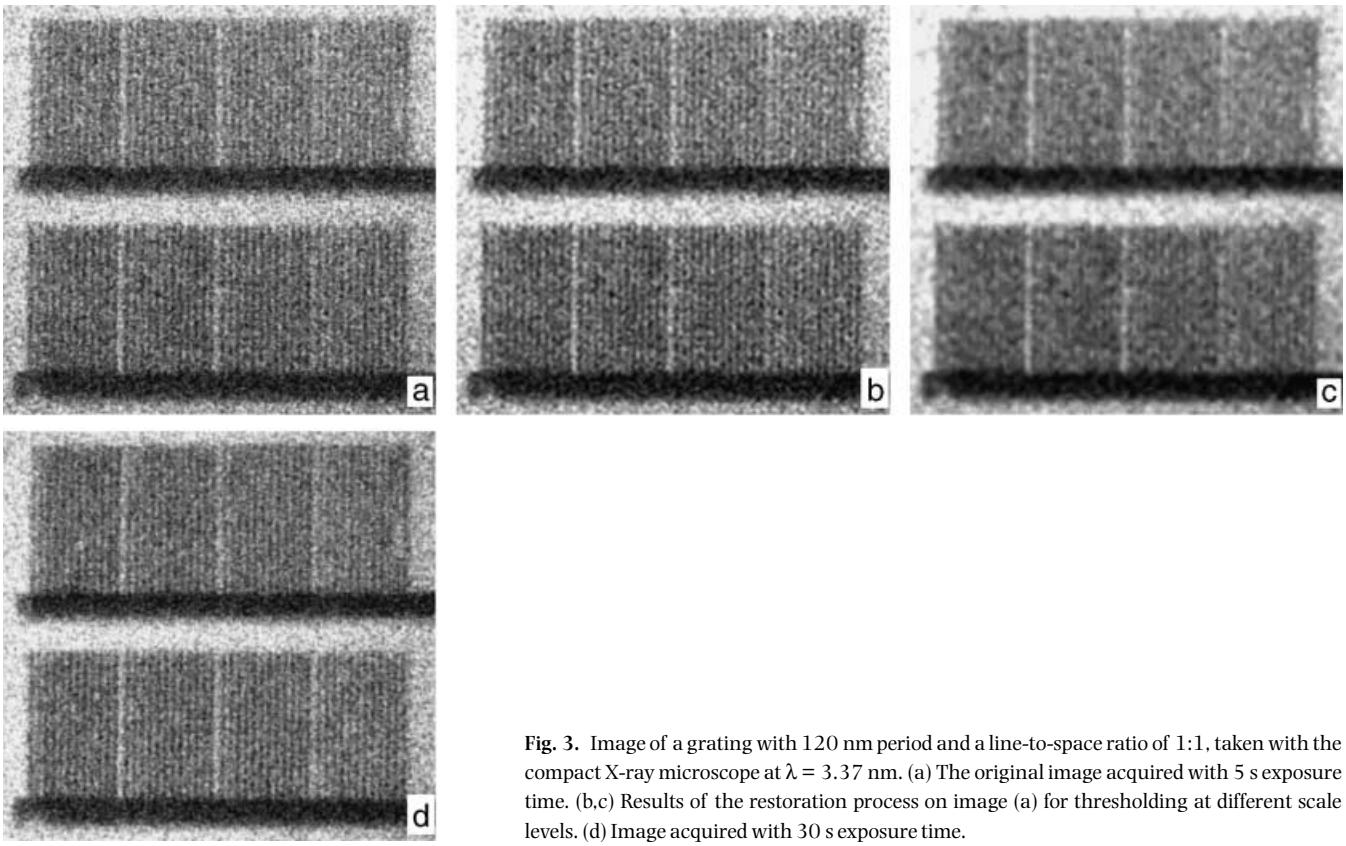

Fig. 3. Image of a grating with 120 nm period and a line-to-space ratio of 1:1, taken with the compact X-ray microscope at $\lambda = 3.37$ nm. (a) The original image acquired with 5 s exposure time. (b,c) Results of the restoration process on image (a) for thresholding at different scale levels. (d) Image acquired with 30 s exposure time.

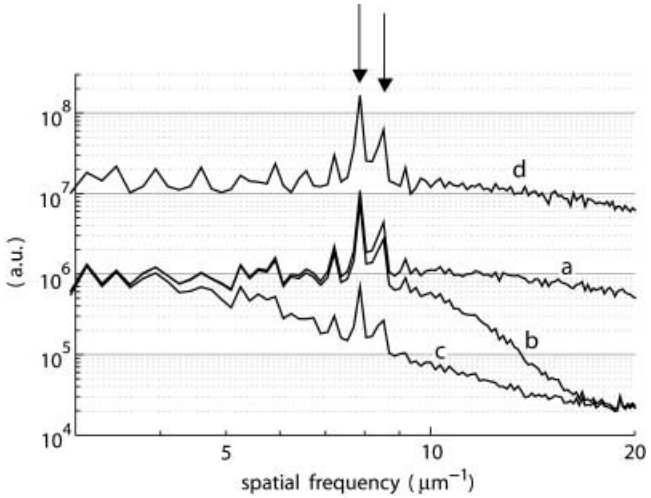

Fig. 4. Power spectra of the gratings in Fig. 3 for different exposure times and restoration steps. (a) Initial image acquired with 5 s exposure time; (b,c) restored images of image (a); (d) original image, obtained after 30 s exposure time. The double peak at the arrows represents the major spatial frequencies of the grating structure (cf. Fig. 3).

around 8 μm^{-1}, whereas the noise level (at higher spatial frequencies) is higher than for the wavelet denoising. The noise level for the Wiener-filtered image using a three-pixel neighbourhood (curve c) is approximately equal to the high-spatial-frequency noise of the wavelet-denoised image, but exhibits a loss of information for the spatial frequencies of interest.

Figure 6 shows a series of images of a diatom. These organisms are unicellular algae generally placed in the family Bacillariophyceae with cell walls made of silica. The smallest structure for the diatoms in use was about 100 nm. Diatoms have a more demanding structure for image restoration than is provided by the gratings. Figure 6(a) shows the original image, averaged over three images obtained with 10 s exposure time with 1000× magnification. Figure 6(b) is the same image after application of the thresholding at the finest scale level. The image on the right shows the same diatom, obtained with 60 s exposure time. Figure 6(b) shows the image enhancement achieved by applying the wavelet algorithm to the image in Fig. 6(a). For comparison, an image of the same diatom in a scanning electron microscope is shown in Fig. 7.

5. Conclusions

The results of the wavelet restoration process indicate that we can enhance image quality. A rough estimate shows that it is possible to lower the exposure time by a factor of 2 without loss of image quality and relevant image information. Applying classical Fourier filtering methods to the same compact X-ray microscope image leads to a significantly inferior result compared with the wavelet-based method. Finally, it should be noted that our algorithm turned out to be more efficient when applied to a few images acquired with a short exposure time and averaging the restored images than when restoring one image recorded with a long exposure time. This is due to the fact that the denoising procedure itself causes artefacts, and the reconstructions are blurred near the edges (Candès & Donoho, 2000). The influence of these artefacts on the final image is minimized by averaging.

Shorter exposure times improve the operability of the current compact X-ray microscope. In addition to the reduction in exposure time due to the wavelet denoising, we expect to

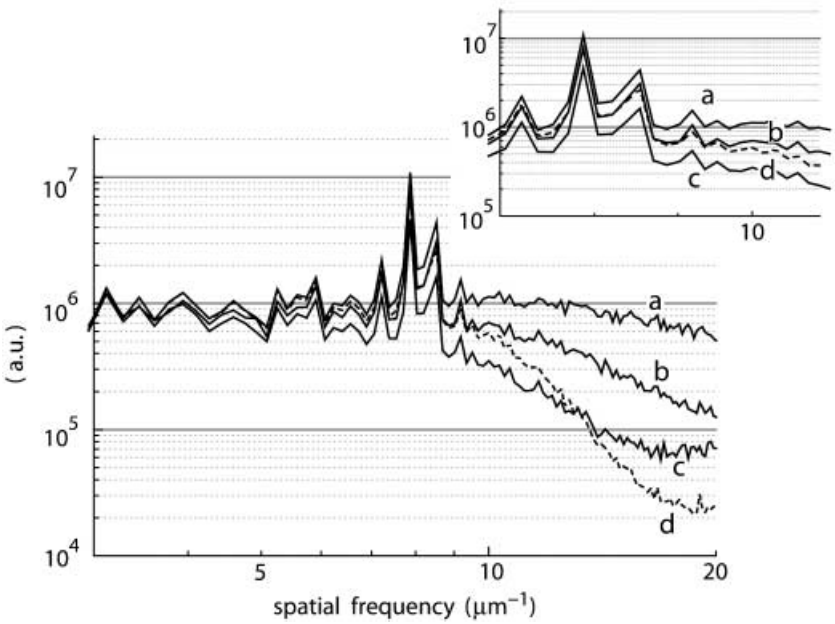

Fig. 5. Power spectra of the gratings in Fig. 3 for different filtering methods: (a) initial image acquired with 5 s exposure time; (b,c) restored images of the initial image using a pixel-wise adaptive Wiener filter; (d) restored image of the initial image using the wavelet filtering at the first scale level. The double peak represents the major spatial frequencies of the grating structure (cf. Fig. 3). For clarity the region around the double peak is enlarged to the upper right.

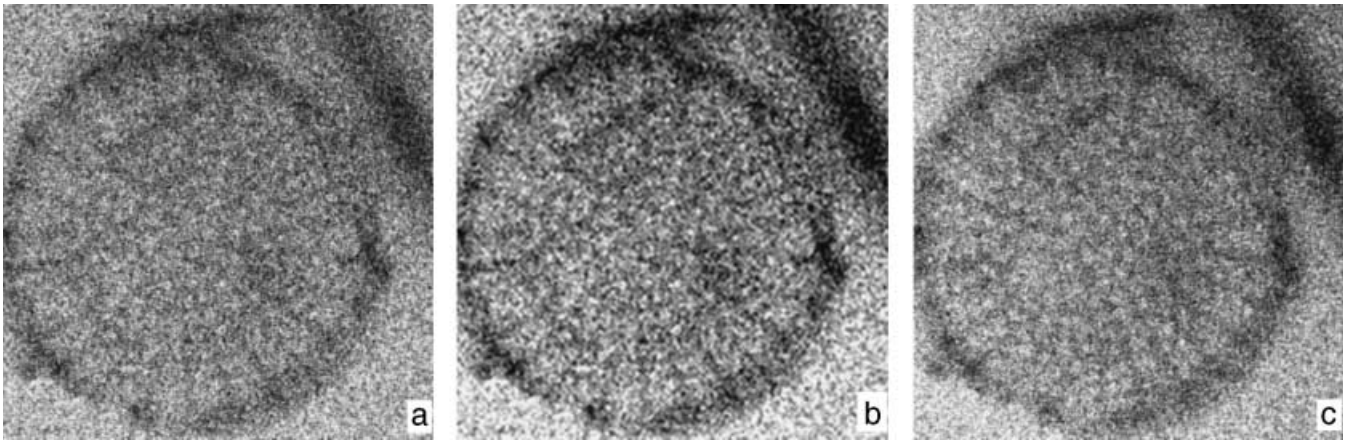

Fig. 6. X-ray micrograph of a diatom, imaged with the compact X-ray microscope at $\lambda = 3.37$ nm. (a) The original image, averaged over three images acquired with 10 s exposure time. (b) Results of the restoration process on image (a) for thresholding at the finest scale. (c) The same diatom with 60 s exposure time.

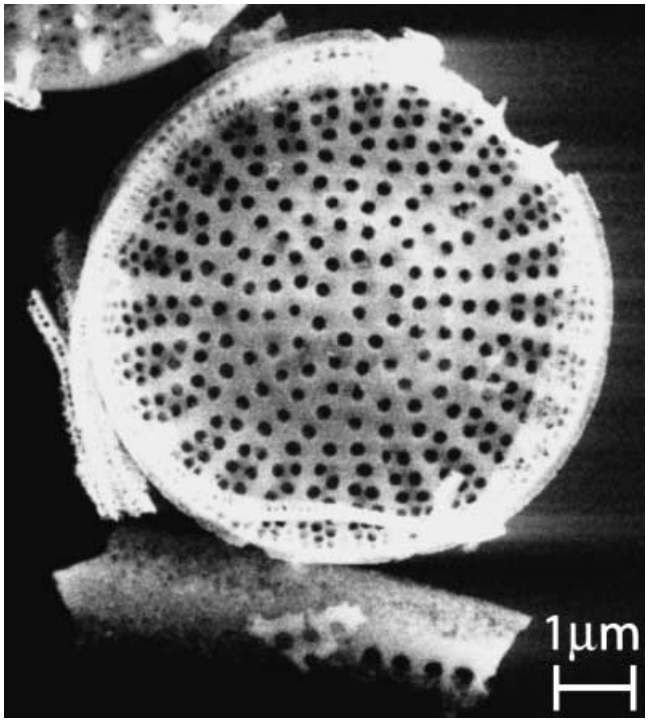

Fig. 7. Image of the diatom, taken with a scanning electron microscope.

reduce the exposure time by improved optics and sources. In the long term, the combination of such improvements potentially allows us to perform wet imaging with exposure times of the order of 1 s (Hertz *et al.*, 2002). This would make compact X-ray microscopy possible with the exposure times of typical bending-magnet synchrotron-based microscopes. Furthermore, denoising resulting in shorter exposure times reduces the radiation dose deposited on the sample, thereby reducing radiation damage on, for example, biological objects. Such a compact microscope would allow high-resolution biological imaging to be performed in the small-scale laboratory.

Acknowledgements

We wish to thank Göran Johansson for experimental help with the compact X-ray microscope and Stefan Rehbein for his assistance in the nanofabrication lab. This work has been supported by the Swedish Research Council.

References

Berglund, M., Rymell, L., Peuker, M., Wilhein, T. & Hertz, H.M. (2000) Compact water-window transmission x-ray microscopy. *J. Microsc.* **197**, 268–273.

Boutet de Monvel, J., Le Calvez, S. & Ulfendahl, M. (2001) Image restoration for confocal microscopy: improving the limits of deconvolution, with application to the visualization of the mammalian hearing organ. *Biophys. J.* **80**, 2455–2470.

Candès, E.J. & Donoho, D.L. (2000) Recovering edges in ill-posed inverse problems: optimality of curvelet frames. *Ann. Statist.* **30**, 784–842.

Donoho, D.L. (1995) De-noising by soft thresholding. *IEEE Transitions on Information Theory*. **41**, 613–627.

Donoho, D.L. & Johnstone, I.M. (1994) Ideal adaption via wavelet shrinkage. *Biometrika*, **81**, 425–455.

Donoho, D.L. & Johnstone, I.M. (1995) Adapting to unknown smoothness via wavelet shrinkage. *J. Am. Stat. Assoc.* **90**, 1200–1224.

Fligge, M. & Solanki, S.K. (1997) Noise reduction in astronomical spectra using wavelet packet. *Astron. Astrophys. Suppl. Series*, **124**, 579–587.

Hertz, H.M., Johansson, G.A., Stollberg, H., de Groot, J., Hemberg, O., Holmberg, A., Rehbein, S., Jansson, P., Eriksson, F. & Birch, J. (2003) Table-top x-ray microscopy: Sources, optics and applications. *J. Phys. IV France*. **104**, 115–119.

Johansson, G.A., Holmberg, A., Hertz, H.M. & Berglund, M. (2002) Design and performance of a laser-plasma-based compact soft x-ray microscope. *Rev. Sci. Instr*. **73**, 1193–1197.

Kirz, J., Jacobsen, C. & Howells, M. (1995) Soft x-ray microscopes and their biological applications. *Quart. Rev. Biophys.* **28**, 33–130.

Lehr, J., Sibarita, J.B. & Chassery, J.M. (1998) Image restoration in x-ray microscopy: PSF determination and biological applications. *IEEE Trans. Image Proc.* **7**, 258–263.

Mallat, S. (1999) *A Wavelet Tour of Signal Processing.* Academic Press, New York.

Schmahl, G., Rudolph, D., Niemann, B. & Christ, O. (1980) Zone-plate x-ray microscopy. *Quart. Rev. Biophys.* **13**, 297–315.

Sibarita, J.B., Chassery, J.M. & Robert-Nicoud, M. (1995) Image restoration applied to x-ray microscopy – Application to images with low signal to noise ratio. *SPIE*, **2329**, 337–347.

Sibarita, J.B., Lehr, J., Chassery, J.M., Robert-Nicoud, M., Guttmann, P. & Schmahl, G. (1998) Image Quality Enhancement in X-Ray Microscopy. *X-Ray Microscopy and Spectromicroscopy* (ed. by J. Thieme, G. Schmahl, D. Rudolph and E. Umbach), pp. I135–I139. Springer-Verlag, Berlin.

Starck, J.L. & Bijaoui, A. (1994) Filtering and deconvolution by the wavelet transform. *Signal Processing*, **35**, 195–211.

Starck, J.L., Bijaoui, A., Lopez, B. & Perrier, C. (1994) Image reconstruction by the wavelet transform applied to aperture synthesis. *Astron. Astrophys.* **283**, 349–360.

Wilhein, T., Hambach, D., Niemann, B., Berglund, M., Rymell, L. & Hertz, H.M. (1997) Off-axis reflecting zoneplate for quantitative soft x-ray source characterization. *Appl. Phys. Lett.* **71**, 190–192.